A method for dynamic system characterization using hydraulic series resistance†

Dongshin Kim,[ab] Naomi C. Chesler[ab] and David J. Beebe*[ab]

Received 1st December 2005, Accepted 2nd March 2006
First published as an Advance Article on the web 20th March 2006
DOI: 10.1039/b517054k

The pressure required to drive flow through a microfluidic device is an important characteristic of that device. We present a method to measure the flow rate through microfluidic components and systems, including micropumps and microvalves. The measurement platform is composed of two pressure sensors and a glass tube, which provides series resistance. The principle of the measurement is the fluid dynamical equivalent of Ohm's law, which defines the relationship between current, resistance, and voltage that are analogues to flow rate, hydraulic resistance, and pressure drop, respectively. Once the series resistance is known, it is possible to compute the flow rate through a device based on pressure alone. In addition, the dynamic system characteristics of the device—resistance and capacitance—can be computed. The benefits of this method are its simple configuration, capability of measuring flow rate accurately from the more easily measured pressure, and the ability to predict the dynamic response of microfluidic devices.

Introduction

Flow rate measurement is essential to characterizing the performance of not only whole systems but also microfluidic components including micropumps and microvalves.[1–7] For low pressure gradient flow (*e.g.*, electrokinetic flow), methods such as current monitoring, micro particle imaging velocimetry (microPIV), and fluorescence monitoring are widely used.[8,9] Commercialized flowmeters are also available for bulk flow rate measurement.[9–11] While they are convenient, most of these methods are not appropriate for microfluidic systems due to their limited response time and high flow rate range.

A typical way to measure the flow rate through a pressure-driven microfluidic system is to collect fluid at the output, measure the volume or mass, and divide by the collecting time. In the laboratory setting, a syringe pump can be used to generate a known flow rate. When combined with a pressure sensor, these techniques provide data on the relationship between flow rate and pressure drop, or device resistance. However, for syringe pumps in particular, fluctuations in flow rate due to the gear backlash and precision limitation of lead screws[12] can decrease the accuracy of the measurement. These errors tend to be especially significant at the low flow rates often used in microfluidic devices. To reduce the error, a source of constant air pressure can substitute for the syringe pump.[11] However, then the fluid again needs to be collected at the outlet port to measure the flow rate for a given pressure. The major limitations of these methods are that they can provide neither instantaneous flow rate for time-varying flows nor information about the dynamic characteristics of a microfluidic device. Understanding the dynamic response of components such as pumps and valves, which facilitate actuation, is critical to evaluating the device performance as a function of the frequency and pressure of actuation.[1,13–15] To date, most discussions of the dynamic response of microfluidic devices have been qualitative rather than quantitative.

Clinicians and physiologists have faced a similar problem: pressure is easier to measure than flow rate, and the dynamic behavior of systems, such as the vasculature, are critical to performance. As early as 1905, a pioneer in the field of hemodynamics, Otto Frank, sought to predict flow rate from pressure measurements.[16] Nearly 50 years later, McDonald[17] and Womersley[18–21] used measurements of both flow rate and pressure to compute the resistance and compliance of the vasculature in order to identify and characterize disease. In this paper, we combine these approaches and present a method to compute the instantaneous flow rate through microfluidic devices based on pressure measurements and to determine the dynamic behavior of microfluidic systems and components.

Theory

Analogues exist between electrical and fluidic circuits. In particular, current, resistance, and voltage are analogous to flow rate, hydraulic resistance, and pressure drop, respectively, as diagrammed in Fig. 1. The hydraulic resistances of the upper (R_{1f}) and lower (R_{2f}) tubes in Fig. 1a correspond to R_1 and R_2 in Fig. 1b, respectively. The distensibility, or compliance, of the upper and lower tubes correspond to C_1 and C_2, respectively; and the pressure drops, ΔP_1, ΔP_2 and ΔP_{1-2}, where $\Delta P_1 = P_1 - P_0$, $\Delta P_2 = P_2 - P_0$ and $\Delta P_{1-2} = P_1 - P_2$, correspond to V_i, V_o and V_{i-o}, respectively. Although current is defined as the amount of electrons passing through a cross-sectional area over a given period of time, which is much

[a]*Department of Mechanical Engineering, University of Wisconsin, 240 Mechanical Engineering, 1513 University Avenue, Madison, WI 53706, USA*
[b]*Department of Biomedical Engineering, University of Wisconsin, 2142 Engineering Centers Building, 1550 Engineering Drive, Madison, WI 53706, USA. E-mail: djbeebe@wisc.edu; Tel: (608) 262-2260*
† Electronic supplementary information (ESI) available: Arbitrary, time-dependent pressure waveform used to validate the flow rate measurement technique (Fig. S1). See DOI: 10.1039/b517054k

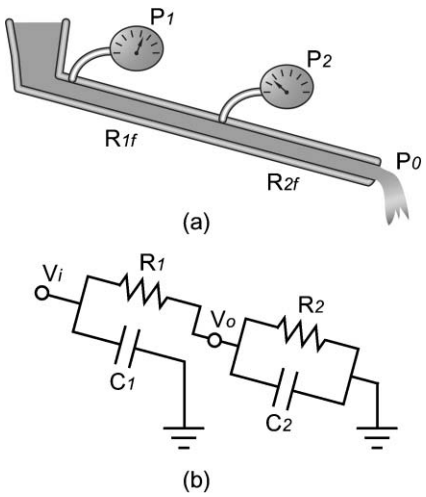

Fig. 1 Fluidic system and electrical analogue. The hydraulic resistances of the upper (R_{1f}) and lower (R_{2f}) tubes in (a) correspond to R_1 and R_2 in (b), respectively. The distensibility, or compliance, of the upper and lower tubes correspond to C_1 and C_2, respectively. The pressure drops, ΔP_1, ΔP_2 and ΔP_{1-2}, where $\Delta P_1 = P_1 - P_0$, $\Delta P_2 = P_2 - P_0$ and $\Delta P_{1-2} = P_1 - P_2$, correspond to V_i, V_o and V_{i-o}, respectively.

like a hydraulic mass flow rate, the volumetric flow rate has been used frequently.[22] Indeed, the governing equation for the hydraulic system is based on Hagen–Poiseuille's law, which assumes the fluid is incompressible (*i.e.*, density does not change over time or space) and thus mass flow rate and volumetric flow rate are interchangeable.

In microchannels, the flow is often laminar (*i.e.*, low Reynolds number). Inertial effects are negligible if the operating frequency is well below the resonance frequency of the flow.[23] Thus, the electrical analogue of inertia, which is inductance, can be ignored. Capacitance, the electrical analogue of compliance, can be ignored if non-compliant tubes (*e.g.*, glass tubes) are used with an incompressible fluid. Then, electrically, for a constant voltage source V_i, R_1 can be determined by measuring V_{i-o} and the current at steady state using Ohm's law. In addition, for a given R_1, R_2 can be found from V_o. The corresponding fluidic terms can be determined in the same manner. That is, for a constant driving pressure P_1, R_{1f} can be found from ΔP_{1-2} and the steady flow rate (Q) from eqn (1). Also, R_{2f} can be obtained from eqn (1) and ΔP_2. Importantly, once R_{1f} is known, Q can be found directly from ΔP_{1-2} such that direct flow rate measurement is no longer required. That is, if the lower part of the circuit is a microfluidic device, its resistance can be determined by measuring only pressures. This simple method can be used to evaluate the nonlinearity of microfluidic systems and components for which the hydraulic resistance is a function of pressure.

$$\Delta P = RQ \tag{1}$$

The real advantage of this approach is for systems operating dynamically. Under dynamic conditions, any compliance that exists in the system will alter the pressure-flow rate relationship. If a non-compliant glass tube is always used in the upper position, then a theoretical solution is available. This configuration, in which one resistor is in series with a resistor and capacitor in parallel, is termed an RC low pass filter. In electronics, the cutoff frequency (f_c) is defined as the frequency at which the power output of a circuit is reduced to one-half. This is equivalent to the frequency where a voltage magnitude change of 3 dB is obtained. f_c is also experimentally found by eqn (2) where t_r is the rise time, or the length of time in which the output response increases from 10% to 90% of its maximum.[24] Once R_{1f} and R_{2f} are found from steady state experiments, the compliance of a microfluidic device can be found by imposing a step change in P_1, calculating the rise time of change in P_2 and then solving eqn (2) for C_{2f}.

$$f_c = \frac{1}{2\pi RC} = \frac{0.35}{t_r} \tag{2}$$

With the resistance and capacitance of a microfluidic device determined, its dynamic response can be predicted for an arbitrary input waveform. For example, if the input signal is sinusoidal and frequency is well below f_c, the output signal (ΔP_2) will be relatively unchanged. In contrast, at frequencies well above f_c, the output signal (ΔP_2) will be attenuated significantly, which means the flow rate will be greatly reduced. If the input signal is composed of pulse shapes, the output signal will be the average of the input signal at frequencies well above f_c.

Experiment

To validate this method, we first measured the resistance of a glass tube acting as a series resistance with no compliance. Then we used the theoretical approach described above to predict flow rate for an arbitrary pressure waveform, measure the resistance and compliance of three microfluidic devices using dynamic step changes in pressure and, finally, predict the dynamic response of a microfluidic system.

The experimental setup is diagrammed in Fig. 2. A compressed, dry nitrogen gas source (a) connected to a regulator (b) was used to pressurize a water column (c). Between the water column (c) and the system outlet were a solenoid valve (d) for controlling pressure, a glass tube (R_{1f}) acting as a series resistance and a microfluidic device (R_{2f}). A function generator (f) (33220A, Agilent, Palo Alto, CA, USA) and controller (e) were used to control the solenoid valve (d) (LHDA1223111H, Lee Company, Westbrook, CT, USA). The series resistance glass tube was 0.5 mm id and 30 cm long. Three microfluidic devices were used; each was a PDMS channel with dimensions as shown in Table 1. Pressure sensors (p_1) upstream and (p_2) downstream (models 142PC30D and 142PC15D, Honeywell, NJ, USA, respectively) of the series resistance, connected *via* T-connectors, were used to measure P_1 and P_2. Pressure data were acquired at 166 Hz and saved on a PC (g) (PCI-1200 and LabView, National Instrument, TX, USA). Large diameter PVC tubes (1.7 mm id and 5 cm long) were used to connect the pressure sensors to the water lines to minimize viscous losses. The system outlet was at atmospheric pressure. Time-averaged flow rate was measured experimentally by collecting water at the outlet (h) for one minute; the sample was weighed using an electronic scale (AB54-S, Mettler Toledo, Columbus, OH, USA).

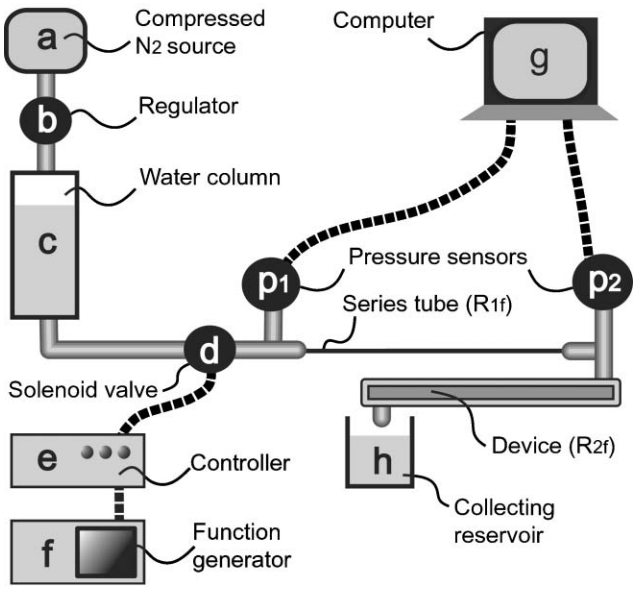

Fig. 2 Schematic of measurement system. A compressed, dry nitrogen gas source (a) connected to a regulator (b) was used to pressurize a water column (c). Between the water column and the system outlet were a solenoid valve (d) for controlling pressure, a glass tube acting as a series resistance and a microfluidic device.

Table 1 Specifications for the microfluidic devices

Category	Device A	Device B	Device C
Width/μm	500	500	1000
Height/μm	240	240	100
Length/mm	274.4	274.4	274.4
Membrane thickness/μm	40	140	100

To determine the series resistance R_{1f}, the pressure drop ΔP_{1-2} was measured for a range of steady flow rates. A resistance value at each flow rate was calculated. R_{1f} was found by best-fit linear regression to these data. To validate this measured series resistance, the theoretical resistance value of a circular tube was calculated assuming Poiseuille flow from:

$$R_f = \frac{128\mu L}{\pi D^4} \quad (3)$$

where μ is fluid viscosity, and L and D are the length and diameter of a circular tube, respectively.

Then, P_1, P_2 and time-averaged flow rate were measured for an arbitrary, time-dependent P_1 waveform. The instantaneous flow rate was calculated according to eqn (1), given R_{1f}, and integrated to obtain a predicted time-averaged flow rate. This procedure was performed with only a series resistance (no microfluidic test device), a series resistance and a glass tube in place of the microfluidic test device and a series resistance and a microfluidic test device (device C in Table 1).

To determine the resistance and compliance of the microfluidic test devices, P_2 was measured for dynamic step changes in P_1. The rise times in ΔP_2 were found for each device for a range of pressure step heights. The theoretical resistance values for the microfluidic test devices were calculated from:

$$R_f = \frac{12\mu L}{wh^3}\left[1 - \frac{h}{w}\left(\frac{192}{\pi^5}\sum_{n=1,3,5}^{\infty}\frac{1}{n^5}\tanh\left(\frac{n\pi w}{2h}\right)\right)\right]^{-1} \quad (4)$$

where w and h are the channel width and height, respectively.[9]

Then, C_{2f} was computed according to eqn (2). Finally, to validate these computed resistance and compliance values, a model for the first order system was created using the MATLAB Simulink. The experimental and model-generated data were compared.

Results and discussion

Series resistance

The constant inlet pressure was well maintained with the experimental setup and a designated level of pressure was easily obtained by adjusting the air pressure regulator. R_{1f}, calculated by the least squares method from experimental data at a range of pressures, was 199.27 kPa s mL^{-1}, which was in close agreement with theoretical value (201.05 kPa s mL^{-1}). Given this value for R_{1f}, time-averaged flow rate through the system was predicted for an arbitrary, time-dependent pressure waveform (see electronic supplementary information (ESI), Fig. S1).† Again, the experimental measurements were in close agreement with the predicted values (Table 2).

Dynamic pressure curve

The responses of the microfluidic devices to dynamic step changes in pressure are shown in Fig. 3. Line P shows the pressure drop across the entire system (ΔP_1) while the other lines indicate the pressure drop across each of the three devices (ΔP_2). Note, line P is unstable at the rising edge of each step (see circled region, Fig. 3). This type of oscillation, or ringing, is typically caused by inductance in a system, which we have assumed to be negligible. Indeed, the Reynolds number under these conditions range from 100 to 1000, which is within the laminar flow regime. To determine the source of the oscillation, a balloon popping test was performed; that is, the dynamic response of the pressure sensor itself was evaluated by applying a step input that is generated when the balloon pops.[25] The result was similar to the ringing in Fig. 3, which suggests that sensor error is responsible. As expected, there was a similar oscillation in ΔP_2 when a glass tube was substituted for the test device. When there was no oscillation region in line P, a bubble inside the system was identified.

Compared to the input waveform, all devices showed delayed rise times. Since R_{2f} of each device was measured in

Table 2 Comparison of measured and predicted time-averaged flow rate for an arbitrary, time-dependent pressure waveform[a]

Flow rate/mL min^{-1}	R only	R + G	R + C
Computed	20.079	6.834	6.621
Measured	20	6.77	6.675
Error (%)	0.4	0.9	0.8

[a] R: Series resistor, G: Non-compliant glass tube, C: Device C.

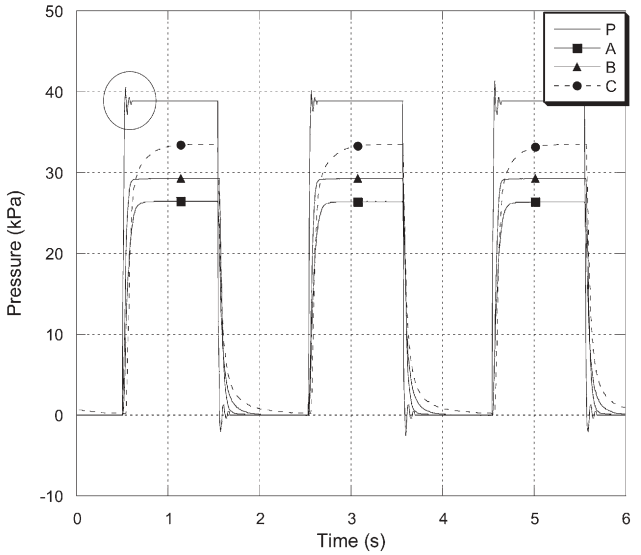

Fig. 3 Response of the system (P) and three microfluidic devices (A, B and C as in Table 1) to dynamic step changes in pressure. All devices showed delayed rise times which could be used to compute the compliance of devices (C_{2f}) according to eqn (2). Note, line P is unstable at the rising edge of each step (see circled region). To determine the source of the oscillation, a balloon popping test was performed[25] and the result suggested that sensor error was responsible.

response to steady flow, the rise time could be used to compute C_{2f} according to eqn (2). Both R_{2f} and C_{2f} were calculated for a range of pressures (Fig. 4 and 5). Device C had higher resistance due to its smaller cross-sectional area (0.1 mm^2 *vs.* 0.12 mm^2 for A and B) and higher aspect ratio (10 *vs.* 2.1 for A and B); the channel aspect ratio is inversely related to the hydraulic radius, a key parameter of flow resistance.[9,26] The decrease in resistance with pressure seen in all devices was caused by the increase in channel cross-sectional area with pressure-induced membrane deformation. Thus, the degree to which the resistance decreased with increasing pressure is an indication (albeit a qualitative one) of device compliance. While device C does not have the thinnest membrane (100 μm *vs.* 40 μm for A and 140 μm for B), it has the largest membrane area (*i.e.*, length times width = 274.4 mm^2 *vs.* 137.2 mm^2 for A and B) and so the rate of change of the resistance was greatest in device C. In confirmation, the compliance of device C was found to be greater than devices A and B by the rise time method (Fig. 5). The compliance of device B, which has the thickest membrane and a membrane area less than or equal to the other devices was less than that of the other devices, as expected.

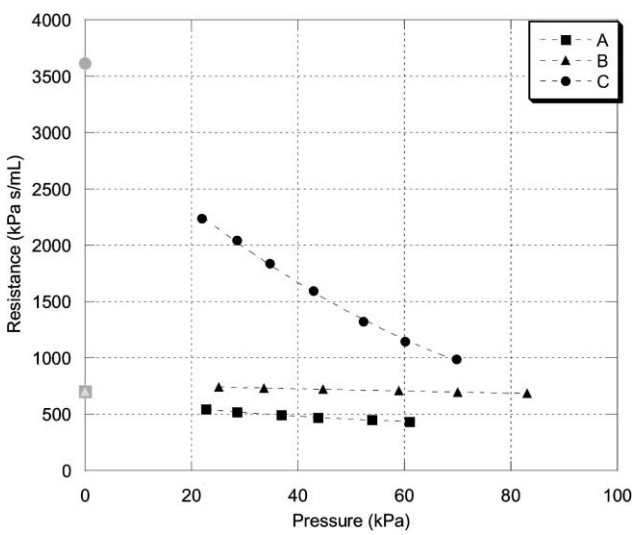

Fig. 4 The calculated resistance of microfluidic devices A, B and C from constant pressure experiments. Gray symbols are theoretical values based on eqn (4). Device C had higher resistance due to its smaller cross-sectional area and higher aspect ratio than other devices. The decrease in resistance with pressure seen in all devices was caused by the increase in channel cross-sectional area with pressure-induced membrane deformation. Thus, the degree to which the resistance decreased with increasing pressure is an indication of device compliance.

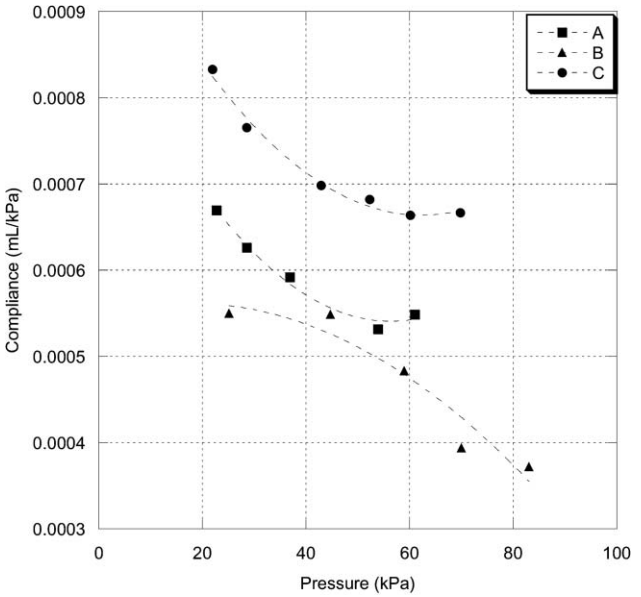

Fig. 5 The calculated compliance of the microfluidic devices A, B, and C from dynamic step change in pressure experiments. The compliance of device C was greater than the other devices because it had a larger membrane area, despite its smaller membrane thickness. The compliance of device B, which had the thickest membrane and a membrane area less than or equal to the other devices was less than that of the other devices, as expected.

Dynamic response and prediction

The dynamic response of device C for different actuation frequencies is shown in Fig. 6; this plot demonstrates that the system behaved like an RC low pass filter with a cutoff frequency of 1.3 Hz at 45 kPa. Note that for frequencies above 1.3 Hz, the amplitude is reduced whereas for frequencies below 1.3 Hz, it is not.

To estimate the effect of the inductance, the resonance frequency was calculated (*i.e.*, $f_0 = 1/\mathrm{sqrt}(LC) \geqslant 20$ Hz) which verified that the experiment was performed well below the resonance frequency. Thus, the effect of the inductance on the current experimental setup can be ignored. Alternatively,

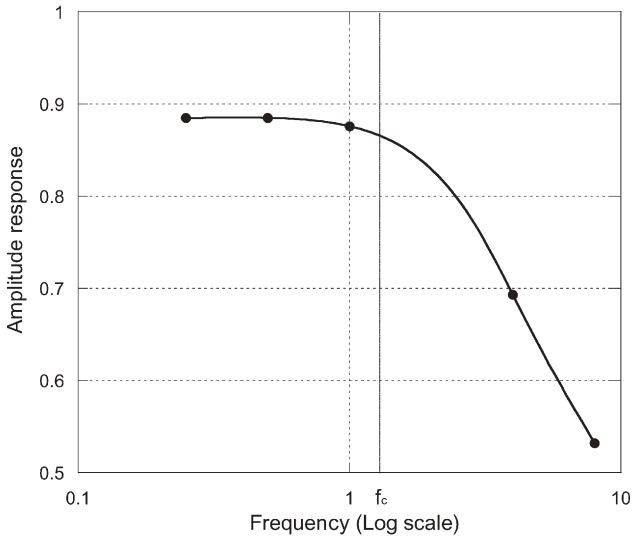

Fig. 6 Dynamic response of a microfluidic system. This plot demonstrates that the system behaved like an RC low pass filter with a cutoff frequency (f_c) of 1.3 Hz. Note that for frequencies above f_c, the amplitude is reduced significantly whereas for frequencies below f_c, it is not.

the critical dynamic Reynolds number can be used to estimate the effect of inductance.[27,28]

Finally, the comparison between the measured data and behavior predicted by a first order RC circuit model using the resistance and compliance values obtained here is shown in Fig. 7. The rise curves match exactly; however, there is some mismatch between the decay curves. Part of the mismatch is likely due to hysteresis in the device since the decay time was slower than the rise time. However, the mismatch could not be eliminated by adjusting the model by the measured decay time. Thus, other factors likely contribute to the decay error,

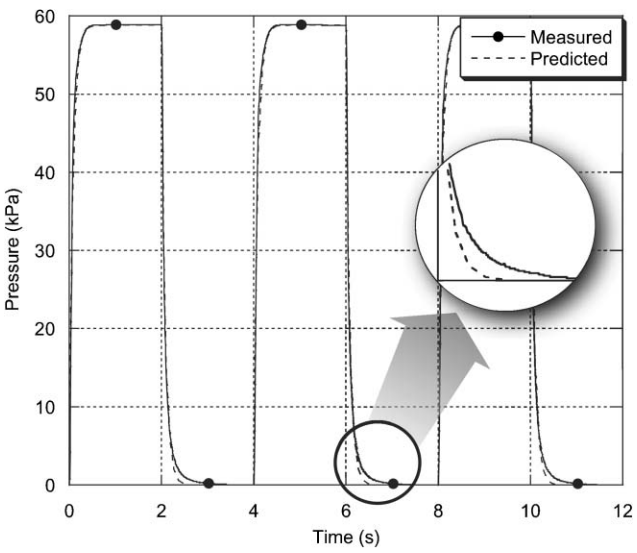

Fig. 7 Comparison between the predicted and measured curves. The rise curves match exactly; however, there is some mismatch between the decay curves (see magnified inset of the decay curve). This mismatch is thought to be caused by hysteresis in the device, geometric non-uniformities and the non-Hookean property of the device.

including geometric non-uniformities and the non-Hookean property of the device; these are beyond the scope of this paper.

Although the experimental setup successfully demonstrated the capability to analyze the dynamic response of microfluidic devices, errors induced by entrance and exit effects, valving, bubbles invisible to the naked eye, and connecting elements may have influenced our results. To increase the accuracy of the system, the system should be devoid of bubbles, use rigid connecting elements, and employ high precision pressure sensors.

Implications

We have presented a simple experimental method for calculating the flow rate through a microfluidic device based on pressure alone and for determining the resistance and compliance of a microfluidic system based on an electrical circuit analogue and electrical circuit theory. Quantifying the resistance and compliance of a microfluidic device, or more generally, the impedance of a device, with simple pressure waveforms allows the device response to arbitrary and more complex waveforms to be accurately predicted. Based on the early work of Frank,[16] McDonald[17] and Womersley,[18–21] impedance analysis is often used to characterize complex fluid networks such as the systemic and pulmonary vasculatures[29–31] and airways.[32,33] Indeed, increasingly impedance analysis is being used clinically since changes in resistance, compliance and inertance can be indications of disease.[33–35] Applying these principles to microfluidic systems provides a more thorough way to characterize components and devices, predict the dynamic response to arbitrary pressure and flow waveforms, and easily detect changes in device characteristics such as resistance and compliance that affect performance.

Acknowledgements

Authors would like to thank Prof. John G. Webster, Dr Javier Atencia and the MMB research group for helpful discussions and the NCFPD for funding.

References

1 M. Hu, H. J. Du, S. F. Ling, Y. Q. Fu, Q. F. Chen, L. Chow and B. Li, A silicon-on-insulator based micro check valve, *J. Micromech. Microeng.*, 2004, **14**, 3, 382–387.
2 Q. Yu, J. M. Bauer, J. S. Moore and D. J. Beebe, Responsive biomimetic hydrogel valve for microfluidics, *Appl. Phys. Lett.*, 2001, **78**, 17, 2589–2591.
3 S. Shoji and M. Esashi, Microflow Devices And Systems, *J. Micromech. Microeng.*, 1994, **4**, 4, 157–171.
4 D. J. Laser and J. G. Santiago, A review of micropumps, *J. Micromech. Microeng.*, 2004, **14**, 6, R35–R64.
5 N.-T. Nguyen, Micro check valves for integration into polymeric microfluidic devices, *J. Micromech. Microeng.*, 2004, **14**, 69–75.
6 T. Q. Truong and N. T. Nguyen, A polymeric piezoelectric micropump based on lamination technology, *J. Micromech. Microeng.*, **14**, 4, 632–638.
7 X.-Q. Wang and Y.-C. Tai, A Normally Closed In-Channel Micro Check Valve, in *13th IEEE International Conference on MEMS, 23–27 Jan 2000*, pp. 68–73.
8 N. Sundararajan, D. S. Kim and A. A. Berlin, Microfluidic operations using deformable polymer membranes fabricated by single layer soft lithography, *Lab Chip*, 2005, **5**, 3, 350–354.

9 D. J. Beebe, G. A. Mensing and G. M. Walker, Physics and Applications of Microfluidics in Biology, *Annu. Rev. Biomed. Eng.*, 2002, **4**, 261–286.
10 S. S. Hsieh, C. Y. Lin, C. F. Huang and H. H. Tsai, Liquid flow in a micro-channel, *J. Micromech. Microeng.*, 2004, **14**, 4, 436–445.
11 D. Liu and S. V. Garimella, Investigation of liquid flow in microchannels, *J. Thermophys. Heat Transfer*, 2004, **18**, 1, 65–72.
12 K. V. Sharp, *Experimental investigation of liquid and particle-laden flows in microtubes*, Thesis, University of Illinois at Urbana-Champaign, IL, USA, 2001.
13 C. Yamahata, F. Lacharme, Y. Burri and M. A. M. Gijs, A ball valve micropump in glass fabricated by powder blasting, *Sens. Actuators, B*, 2005, **110**, 1, 1–7.
14 N. L. Jeon, D. T. Chiu, C. J. Wargo, H. K. Wu, I. S. Choi, J. R. Anderson and G. M. Whitesides, Design and fabrication of integrated passive valves and pumps for flexible polymer 3-dimensional microfluidic systems, *Biomed. Microdevices*, 2002, **4**, 2, 117–121.
15 M. L. Adams, M. L. Johnston, A. Scherer and S. R. Quake, Polydimethylsiloxane based microfluidic diode, *J. Micromech. Microeng.*, 2005, **15**, 8, 1517–1521.
16 W. W. Nichols and M. F. O'Rourke, *McDonald's blood flow in arteries: theoretical, experimental, and clinical principles*, Oxford University Press, New York, 5th edn, 2005, **vol. 1**, p. 607.
17 D. A. McDonald, The relation of pulsatile pressure to flow in arteries, *J. Physiol.*, 1955, **127**, 3, 533–52.
18 J. R. Womersley, Method for the calculation of velocity, rate of flow and viscous drag in arteries when the pressure gradient is known, *J. Physiol.*, 1955, **127**, 3, 553–63.
19 J. R. Womersley, Oscillatory flow in arteries: effect of radial variation in viscosity on rate of flow, *J. Physiol.*, 1955, **127**, 2, 38–9P.
20 J. R. Womersley, Mathematical theory of oscillating flow in an elastic tube, *J. Physiol.*, 1955, **127**, 2, 37–8P.
21 J. R. Womersley, Oscillatory flow in arteries: the constrained elastic tube as a model of arterial flow and pulse transmission, *Phys. Med. Biol.*, 1957, **2**, 2, 178–87.
22 V. C. Rideout, *Mathematical and Computer Modeling of Physiological Systems*, Prentice-Hall, Englewood Cliffs, NJ, 1991, p. 261.
23 T. Bourouina, A. Bosseboeuf and J. P. Grandchamp, Design and simulation of an electrostatic micropump for drug-delivery applications, *J. Micromech. Microeng.*, 1997, **7**, 186–188.
24 W. D. Stanley, *Electronic Devices*, Prentice-Hall, Englewood Cliffs, NJ, 1989, p. 810.
25 R. A. Peura, *Medical instrumentation (Application and design)*, ed. J. G. Webster, John Wiley & Sons, Inc, United States, 3rd edn, 1998, **vol. 1**, p. 302.
26 R. B. Bird, W. E. Stewart and E. N. Lightfoot, *Transport Phenomena*, John Wiley & Sons, New York, 2001.
27 X. G. Tang and P. Cheng, Correlations Of The Cycle-Averaged Nusselt Number In A Periodically Reversing Pipe-Flow, *Int. Commun. Heat Mass Transfer*, 1993, **20**, 2, 161–172.
28 C. J. Morris and F. K. Forster, The correct treatment of harmonic pressure-flow behavior in microchannels, *Micro Electro Mech. Syst., Int. Conf.*, 2000, **vol. MEMS-2**, pp. 473–479.
29 J. K.-J. Li, *The arterial circulation: physical principles and clinical applications*, Humana Press, Totowa, NJ, 2000.
30 W. R. Milnor, *Hemodynamics*, Williams & Wilkins, Baltimore, 2nd edn, 1989, ch. XII, p. 419.
31 H. A. Tuchscherer, E. B. Webster and N. C. Chesler, Pulmonary vascular resistance and impedance in isolated mouse lungs: Effects of pulmonary emboli, *Ann. Biomed. Eng.*, DOI: 10.1007/s10439-005-9050-z.
32 D. A. Kaminsky, C. G. Irvin, L. Lundblad, H. T. Moriya, S. Lang, J. Allen, T. Viola, M. Lynn and J. H. Bates, Oscillation mechanics of the human lung periphery in asthma, *J. Appl. Physiol.*, 2004, **97**, 5, 1849–58.
33 D. MacLeod and M. Birch, Respiratory input impedance measurement: forced oscillation methods, *Med. Biol. Eng. Comput.*, 2001, **39**, 5, 505–16.
34 J. L. Izzo, Jr., Arterial stiffness and the systolic hypertension syndrome, *Curr. Opin. Cardiol.*, 2004, **19**, 4, 341–52.
35 H.O. Ventura, S. J. Taler and J. E. Strobeck, Hypertension as a hemodynamic disease: the role of impedance cardiography in diagnostic, prognostic, and therapeutic decision making, *Am. J. Hypertens.*, 2005, **18**, 2, 26S–43S.